Electrostatic forces acting on tip and cantilever in atomic force microscopy

Elmar Bonaccurso,[1,*] Friedhelm Schönfeld,[2] and Hans-Jürgen Butt[1]

[1] *Max-Planck Institute for Polymer Research, Ackermannweg 10, 55128 Mainz, Germany*

[2] *Institute of Microtechnology Mainz, Carl-Zeiss-Strasse 18-20, 55129 Mainz, Germany*

(Received 5 September 2005; revised manuscript received 2 May 2006; published 18 August 2006)

In this paper we quantitatively compare different electrostatic models, which describe the interaction between the tip of an electrically biased atomic force microscopy cantilever and a conducting flat substrate. The models by Hudlet *et al.* [Eur. Phys. J. B **2**, 5 (1998)] and Colchero *et al.* [Phys. Rev. B **64**, 245403 (2001)] provide excellent descriptions of the experimental force, for tip parameters close to their typical values, although an accurate treatment of the electrostatic force contribution due to the cantilever is still missing. We introduce it here, together with a correction function which accounts for the tilting angle between the cantilever and surface, and confirm it with several experiments. Since the electrostatic force acting between a cantilever and a surface can be accurately tuned, force measurements with a defined voltage are also suitable for calibrating cantilever spring constants.

DOI: 10.1103/PhysRevB.74.085413 PACS number(s): 68.37.Ps, 07.79.Lh

I. INTRODUCTION

Electric forces govern many physical and chemical processes and, correspondingly, many technological applications are based on them. For pursuing the next step towards miniaturization, namely nanotechnology, the ability of understanding and making use of electrostatic interactions between nanoscopic elements is paramount. In the last decade progress in this field has been significant. Part of this progress has been driven by the development of the scanning tunneling microscope[1] and the atomic force microscope[2] (AFM), which allows us not only to image and to characterize surfaces, but also to manipulate them on a nanometer and even an atomic scale.[3] The AFM has shown to be a versatile instrument for the measurement of surface forces, and among those also electrostatic forces. When electrostatic forces dominate the total interaction in an AFM, one generally speaks of electrostatic force microscopy (EFM). EFM has been used to image properties of semiconductors,[4,5] local surface potentials,[6] and surface charges,[7,8] electric properties of organic and inorganic integrated circuits,[9] and surface polarization forces.[10] The ability of applying a potential to the sharp tip of an AFM cantilever has been used as a powerful nanolithography tool for structuring several types of surfaces.[11,12]

The electrostatic interaction on a 10 nm scale is the one with the highest strength, as well as the longest range compared to other relevant molecular forces, such as van der Waals or other so-called "chemical" forces.[13] Several papers have advanced our understanding of the electrostatic interaction between an AFM cantilever and a surface.[14–26] Numerical approaches for modeling the electrostatic force have been proposed, among others, by Belaidi *et al.*[18] The authors present a thorough discussion of their model, and compare it with two experimental force curves.[27] So we believe that more experiments are needed to confirm their results. An elegant analytical model was presented by Hudlet *et al.*,[19] where the authors model the tip as a cone with a spherical apex, although they do not consider the contribution of the cantilever. An experimental force curve is compared to their calculations, but the spring constant of the cantilever was not calibrated. Law and Rieutord[24] go a step further, and incorporate also the cantilever contribution into the force calculations. In order to fit their data they introduce a so-called "background force," and add it to the electrostatic force. This contribution is a constant, i.e., not-voltage and not-distance dependent.

The purpose of the present paper is to add a further piece to the puzzle, accounting for the tip and for the cantilever. Special consideration is devoted to the dissimilar effect of the electrostatic force when it interacts with the tip (a quasipunctual load) and with the cantilever (a distributed load), causing bendings described by polynomials of different orders (more details will be given in Sec. II). A large number of measurements have been carried out, by changing the properties of the cantilever, of the tip, of the sample surface, and some environmental parameters. Finally we will also show that the accurately tunable electrostatic force is well suited for calibrating the spring constant K of cantilevers. The quantitative determination of K is the indispensable parameter for obtaining quantitative informations on the magnitude of interactions in AFM and force spectroscopy experiments. Several techniques have been suggested and are applied (for a review see Ref. 28). These techniques are, however, technically demanding, limited in their range of applicability, and a quantitative analysis is difficult. Therefore, any simple, accurate, and reliable method would be welcome.

II. THEORY

The AFM cantilever and the attached tip (Fig. 1), both at potential V_0 with respect to the grounded sample surface, form a capacitor of complex geometry when they are brought in close vicinity to the surface. The force on the tip-cantilever system has the form

$$F = \pi\varepsilon_0 V_0^2 g(z), \tag{1}$$

where ε_0 is the vacuum permittivity and $g(z) \propto dC/dz$ is related to the change of the capacitance C with respect to the separation z between cantilever and surface. The term $g(z)$

 ©2006 The American Physical Society

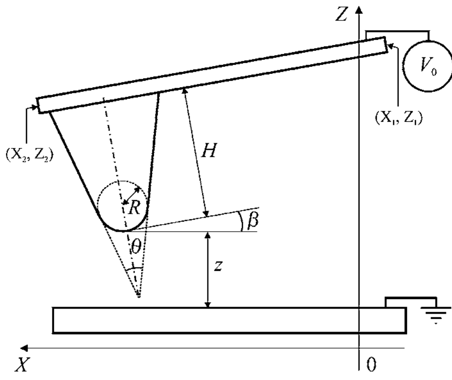

FIG. 1. Scheme of the tip-cantilever-surface setup. The surface is flat and grounded, the cantilever is inclined with respect to the surface by an angle β and is set at a potential V_0. The tip is modeled as a truncated conus of height H and half-angle θ, with a spherical apex of radius R at the end.

depends on the geometry of the tip (apex radius R, half-tip angle θ, and tip height H) and of the cantilever (length L, width w, and inclination angle β).

A. Force on the cantilever

Belaidi *et al.*,[18] Colchero *et al.*,[23] and Law and Rieutord[24] provide similar equations for the electrostatic force acting on a tilted cantilever (see Fig. 1), which are deduced from the equation of a plate capacitor, by neglecting border effects. The distance of the cantilever from the surface depends on x and is given by $Z(X)=z+H\cos\beta+L\sin\beta-X\tan\beta$. Calling $B(X)$ the function describing the width of the cantilever, the factor $g(z)$ is

$$g_{CL}=-\frac{1}{2\pi}\int_{X1}^{X2}\frac{B(X)dX}{Z(X)^2}. \tag{2}$$

By convention, the negative sign indicates an attractive force. In the case of a rectangular cantilever, $B(X)$ is simply the width w of the cantilever.

B. Force on the tip

Law and Rieutord[24] recap equations from former authors[15,17–20,23,29] for the electrostatic force acting on the tip of a cantilever, considering three cases of tips with rotational symmetry: hemispherical apex, cone with spherical apex, and hyperboloid:

$$g_{sphere}=-\frac{R}{z}, \tag{3}$$

$$g_{cone}=-\left\{\frac{1}{\ln^2(\tan\theta/2)}\left[\ln\left(\frac{H}{z+R(1-\sin\theta)}\right)-1+\frac{R\cos^2\theta/\sin\theta}{z+R(1-\sin\theta)}\right]+\frac{R^2(1-\sin\theta)}{z[z+R(1-\sin\theta)]}\right\}, \tag{4}$$

$$g_{hyperboloid}=-\frac{1}{\ln^2(\tan\theta/2)}\left[\ln\left(1+\frac{L}{z}\right)-\frac{\left(\frac{z-R}{\tan^2\theta}\right)H}{z(L+z)}\right]. \tag{5}$$

The total resulting electrostatic force is assumed to be the sum of the cantilever, the tip, and the apex contribution, each one being predominant at a different surface-cantilever separation (for details see Belaidi *et al.*[18]).

C. Taking the calibration of cantilever deflection into account

In commercial AFMs the inclination, and not the deflection, is measured at the end of the cantilever by the optical lever technique. Inclination is usually converted to a deflection by pushing the end of the cantilever upwards by a defined distance using the piezoscanner of the AFM. This is justified by the fact that this is similar to what happens to the cantilever when it is used for imaging and/or force spectroscopy experiments: a concentrated load pushes, or pulls, on the tip. As a result, if we apply a force F_{TIP} at its end, the shape of a rectangular cantilever is described by a third order polynomial:

$$Z_{conc}(X)=\frac{F_{TIP}}{2EI}\left(LX^2-\frac{X^3}{3}\right), \tag{6}$$

where E is the elastic modulus of the material, $I=wt_c^3/12$ is the geometric moment of inertia, and t_c is the thickness of the cantilever. Deflection $Z_{conc}(L)$ and inclination $dZ_{conc}/dX(X=L)$ are related by[30]

$$\frac{dZ_{conc}}{dX}(L)=\frac{3}{2L}Z_{conc}(L). \tag{7}$$

The subscript "conc" indicates that a concentrated force acts at the end of the cantilever.

This is not a problem in "standard" AFM setups where a concentrated force acts on the cantilever tip, since the calibration procedure for obtaining the deflection is as well done by pushing the tip.[31] The situation is different in the case of electrostatic forces, which affect the tip as a concentrated load, but at the same time affect the cantilever as a uniformly distributed load. The shape of the bent cantilever has to be recalculated, the usual calibration procedure has to be modified, and a correction factor has to be determined.

To calculate the correction, we first consider for simplicity a rectangular cantilever, clamped on one end and oriented horizontally to a planar surface ($\beta=0$) at a distance Z_0. Then we extend the analysis to the general case of an inclined cantilever ($\beta>0$), as shown in Fig. 1.

When a voltage is applied, the cantilever bends towards the surface. We assume that this bending is small ($\Delta Z=Z_0-Z\ll Z_0,L$). Since the electrostatic force is homogeneously distributed over the whole length of the cantilever (except for the end with the tip) and depends on the distance between the cantilever and surface, the force affecting the cantilever per unit length is $f=F_{CL}/L=f^*/Z_0^2$. Then its shape is described by a fourth order polynomial,[32,33]

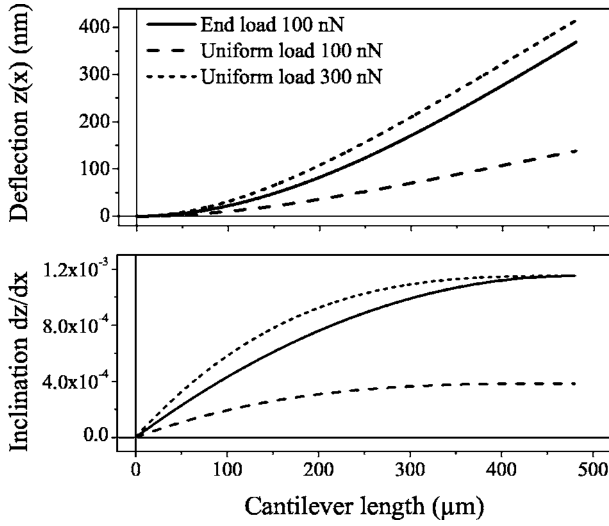

FIG. 2. Calculated deflection and inclination of a rectangular silicon cantilever (L=480, w=50 μm, t_c=2 μm, E=180 GPa) with an end load at the tip, and with two uniform loads on the whole cantilever.

$$Z_{unif}(X) = f\frac{X^2(6L^2 - 4XL + X^2)}{24EI}. \tag{8}$$

The subscript "*unif*" indicates that $Z_{unif}(X)$ describes the bending of a cantilever with a uniformly distributed force per unit length acting on it.

We calibrate each force curve according to the concentrated load model by measuring the inclination at the end of the cantilever, but the electrostatic force bends the cantilever according to the uniform load model. So we need to equate the two inclinations at the end of the cantilevers, $dZ_{conc}/dX(X=L)=dZ_{unif}/dX(X=L)$, in order to be able to relate the effects of the two forces to the bending of the cantilever.

With

$$\frac{dZ_{conc}}{dX}(X=L) = \frac{F_{TIP}L^2}{2EI} \tag{9}$$

and

$$\frac{dZ_{unif}}{dX}(X=L) = \frac{F_{CL}L^2}{6EI} \tag{10}$$

we obtain

$$F_{TIP} = \frac{1}{3}F_{CL} \tag{11}$$

which means that a uniform force three times larger than the one affecting the tip is needed in order to cause the same inclination at the end of the cantilever. This is demonstrated for one example in Fig. 2. For correctly fitting the experimental data with the analytic models, we thus need to place a correction factor $h=\frac{1}{3}$ in front of the contribution of the cantilever in Eq. (2):

$$F_{CL} = -h\frac{\varepsilon_0 V_0^2}{2}\int_{X1}^{X2}\frac{B(X)dX}{Z(X)^2} \tag{12}$$

while the contributions due to the tip and the apex are unchanged, and the sum of all three provides the total electrostatic force. The case of a triangular cantilever should not present a substantial variation in the absolute value of the correction factor. In fact, according to Sader,[34] the bending of a triangular cantilever is equivalent to the bending of cantilever which has its skewed rectangular arms replaced by a single unskewed rectangular plate.

For the general case with $\beta > 0$, the distribution of forces along the lever changes with tip-sample distance, so, unlike in the β=0 case, we will not find a constant conversion factor h, but rather a conversion function $h(Z_0,L,\beta)$.

The force per unit length can be written as $f = F_{CL}/(L\cos\beta) = f^*/(Z_0-Z)^2$. The torque due to the electrostatic force is

$$M = \int_X^{L'}(X' - X)f\,dX' = f^*\int_X^{L'}\frac{X' - X}{(Z_0 - Z)^2}dX' \tag{13}$$

with $L'=L\cos\beta$. The torque due to elastic response of the cantilever is[35]

$$M = EI\cos^3\beta\frac{d^2Z}{dX^2}, \tag{14}$$

where the cosine term is due to the transformation from the coordinate system aligned with the cantilever to the rotated coordinate system (X,Z) shown in Fig. 1. Equations (13) and (14) lead to the integrodifferential equation

$$\frac{d^2Z}{dX^2} = f^*\frac{1}{EI\cos^3\beta}\int_x^{L'}\frac{X' - X}{[Z_0 - Z(X')]^2}dX' \tag{15}$$

with the boundary conditions $Z(X=0)=0$ and $dZ/dX(X=0) = \tan\beta$. Equation (15) can be casted into a fourth order differential equation, which has to be solved by an iterative quadrature procedure due to the involved boundary condition for $Z^{(3)}(X=0)$. Yet, in order to derive an analytical solution we assume the electrostatic force to be sufficiently below the pull-in value and $Z(X')$ in the kernel of Eq. (15) is replaced by the linear term. Using a dimensionless length coordinate and deflection ($x=X/L'$, $z=Z/L'$) we get

$$\frac{d^2z}{dx^2} = f^*\frac{L'}{EI\cos^3\beta}\int_x^1\frac{x' - x}{(z_0 - x'\tan\beta)^2}dx'. \tag{16}$$

Integrating Eq. (16) twice the inclination at the end of the cantilever (x=1) is found to be

$$\frac{dz}{dx}(x=1) = f^*\frac{L'}{EI}\frac{1}{2\sin^3\beta}\left\{\frac{\tan\beta(\tan\beta - 2z_0)}{\tan\beta - z_0} + 2z_0\log\left(1 - \frac{\tan\beta}{z_0}\right)\right\} + \tan\beta. \tag{17}$$

The electrostatic force experienced by the cantilever is, cf. Eq. (13)

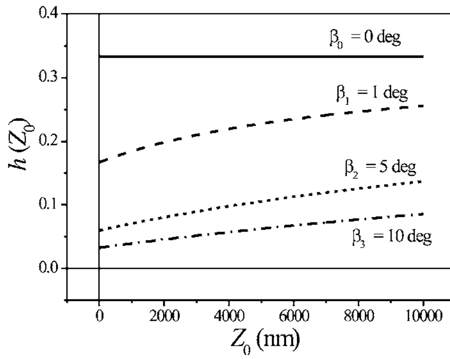

FIG. 3. Calculated conversion functions $h(Z_0,L,\beta)$ plotted versus the separation from the surface Z_0. A rectangular cantilever ($L=480$, $w=50\ \mu$m, $t_c=2\ \mu$m, $E=180$ GPa) having a 4 μm long tip at its end was assumed. Four values of the tilting angle β were assumed: 0°, 1°, 5°, and 10° (curves from top to bottom).

$$F_{CL}=f^*\int_0^{L'}\frac{1}{(Z_0-X'\tan\beta)^2}dX'=f^*\frac{L'}{Z_0^2-Z_0L'\tan\beta}. \tag{18}$$

Rewriting the inclination in Eq. (17) in terms of the electrostatic force in dimensional coordinates yields

$$\frac{dZ_{distr}}{dX}(X=L')=\frac{F_{CL}L'^2}{2EI}h(Z_0,L',\beta)+\tan\beta \tag{19}$$

with

$$h(Z_0,L',\beta)=\frac{Z_0}{L'^3\sin^3\beta}\left\{(2Z_0-L'\tan\beta)L'\tan\beta+2Z_0(Z_0-L'\tan\beta)\log\left(1-\frac{L'\tan\beta}{Z_0}\right)\right\}. \tag{20}$$

The subscript *distr* denotes the case of having a distributed, but not uniform, load along the cantilever. Again, we need to equate the two inclinations at the end of the cantilevers, $dZ_{conc}/dX(X=L')=dZ_{distr}/dX(X=L')$, in order to be able to relate the effects of the two forces on the bending of the cantilever, and we obtain

$$F_{TIP}=h(Z_0,L',\beta)F_{CL}. \tag{21}$$

In the limit of vanishing inclination we find

$$\lim_{\beta\to 0}h(Z_0,L',\beta)=\frac{1}{3}. \tag{22}$$

Thus Eq. (10), the case of a uniform load distribution, is recovered.

Four plots of the conversion function $h(Z_0)$ are presented in Fig. 3, each plot was calculated using a different tilting angle β of the cantilever with respect to the surface. A rectangular cantilever with a length of 480 μm, a width of 50 μm, and having a 4 μm long tip at its end was assumed.

III. EXPERIMENTS

A particle interaction apparatus,[36] equipped with a piezoscanner (P753.11C, Physik Instrumente GmbH, Germany)

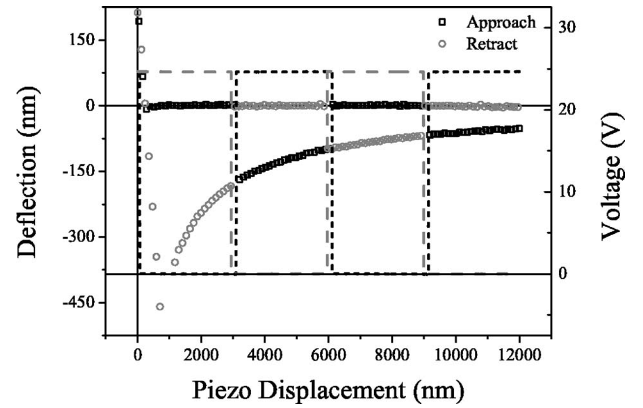

FIG. 4. Deflection versus piezo extension curve (triangular dots) acquired by applying a rectangular half-wave voltage (dashed lines) to a triangular cantilever with pyramidal tip. The piezo was scanned at 1 Hz, the applied voltage had a frequency of 4 Hz.

with a 12 μm scan range, was used to measure cantilever deflection versus piezodisplacement curves at various cantilever-surface voltages, ranging from 0 to about 100 V. Force curves were calculated by multiplying the cantilever deflection with the spring constant of the cantilever to obtain the force, and by adding piezodisplacement and cantilever deflection to obtain the separation. The applied voltage was generated by a function generator (TCE-7704, Toellner GmbH, Germany) and amplified by a homemade HV generator. It was a rectangular half-wave, ranging from 0 to $\pm V_0$, in order to have an internal reference at 0 V, i.e., cantilever and surface at the same voltage, in each force curve (Fig. 4). The frequency of the applied voltage was at least four times higher than the repetition rate of the force curves. Therefore, it was possible to acquire a complete force curve (with approach and retract part), and the baseline at zero potential during a single force scan. On the other hand, the frequency was always much lower than the resonance frequency of the cantilever.

Two types of cantilevers were mainly used: Rectangular silicon cantilevers with a quasiconical tip (PointProbe, NanoWorld GmbH, Germany), and triangular silicon nitride cantilevers, with or without a pyramidal tip (DNP, Veeco Instruments, USA) (Fig. 5). The Young's moduli are $E_{Si}=180$ GPa and $E_{Si3N4}=146$ GPa, respectively. The first are uncoated and are manufactured from highly doped, single crystalline, highly conductive silicon (resistivity about 0.01–0.025 Ω cm for avoiding electrostatic charging. The second are coated with a 15 nm Cr plus 60 nm Au layer, on both sides for avoiding mechanical stresses. Cantilevers and tips were all imaged in a low-voltage mode with a scanning electron microscope (SEM) (LEO 1530 Gemini, Zeiss-LEO GmbH, Germany) for a precise characterization of the tip radii. Dimensions and spring constant of the cantilevers are specified for each measurement in the figure captions. Cantilever spring constants were calibrated with the MFP-1D (Asylum Research, USA) applying the thermal noise method.[37,38] Two substrates were mainly used: A polished silicon wafer with the silicon cantilevers, and a Cr/Au coated glass microscope slide with the coated silicon nitride cantilevers.

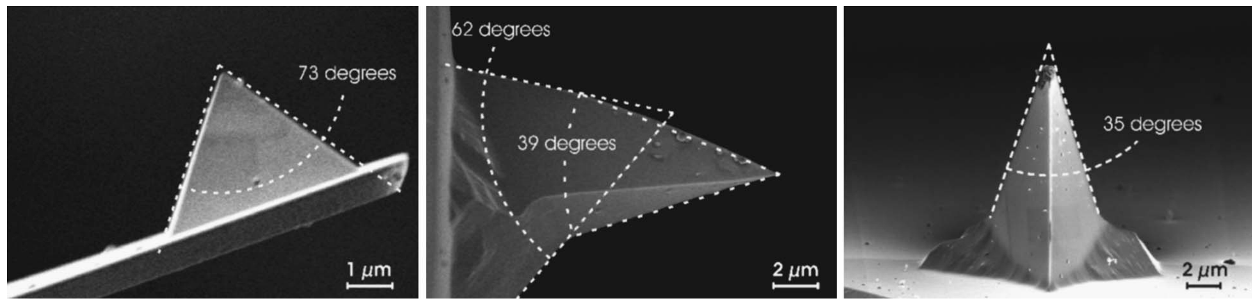

FIG. 5. SEM images of cantilever tips. Left side: pyramidal, gold coated tip on a triangular cantilever. Tip height is 3 μm, half-cone angle is 36.5°. Middle: Side view of a quasiconical tip on a rectangular cantilever. Tip height is 15 μm, upper half-cone angle is 19.5°, lower half-cone angle is 31°. Right side: Front view of a similar tip, the half-cone angle from the front is 17.5°.

Experimental conditions were changed during some force measurements, in particular the influence of relative humidity (RH) was investigated. To do so, the whole setup was placed under a flexible glove box (GloveBag, I^2R, USA), which was then flooded with dry and humid air to achieve RHs between about 5% and 65%.

IV. RESULTS AND ANALYSIS

A. Dependence on applied voltage and cantilever correction function *h*

The voltage dependence is presented in a set of six force curves in Fig. 6. On the left side is shown that a higher voltage causes a larger attractive force between cantilever and surface. On the right side the absolute data were normalized by the square of the voltage, and plotted on a log/log scale, though the forces remain attractive. From this representation the V_0^2 dependence becomes evident, since all curves collapse onto one master curve. The log/log representation was chosen because it better represents the contributions of the apex, tip, and cantilever to the total force as changes in the slope of the curve. Law and Rieutord[24] mention that the way of applying the voltage during a measurement, for example, by an increasing or a decreasing series, affects the V_0^2 dependence, because after an increasing series a residual charge or potential remains on the cantilever. We could not observe such a behavior. Law and Rieutord[24] also observe a repulsive force between the cantilever and surface at separations smaller than 300 nm, and ascribe it to residual charges of equal sign residing on cantilever and surface. We could not observe such repulsive forces between tips and surfaces at any separation, when both were at the same potential. At small separations we only observed attractive forces of the van der Waals type. We could also observe no deviations from the V_0^2 dependence by either changing RH or the temperature, or by applying voltages of positive or negative sign.

The relevance of the correction factor h, or better of the correction function $h(Z_0, L', \beta)$, which considers the cantilever contribution, is demonstrated in Fig. 7. In the upper graph we show experiments where we used a tipless triangular cantilever. The force curves were acquired at three different voltages, and they illustrate the V_0^2 dependence. The solid line shows the calculation of the force according to Eq. (21), all parameters being determined from optical micros-

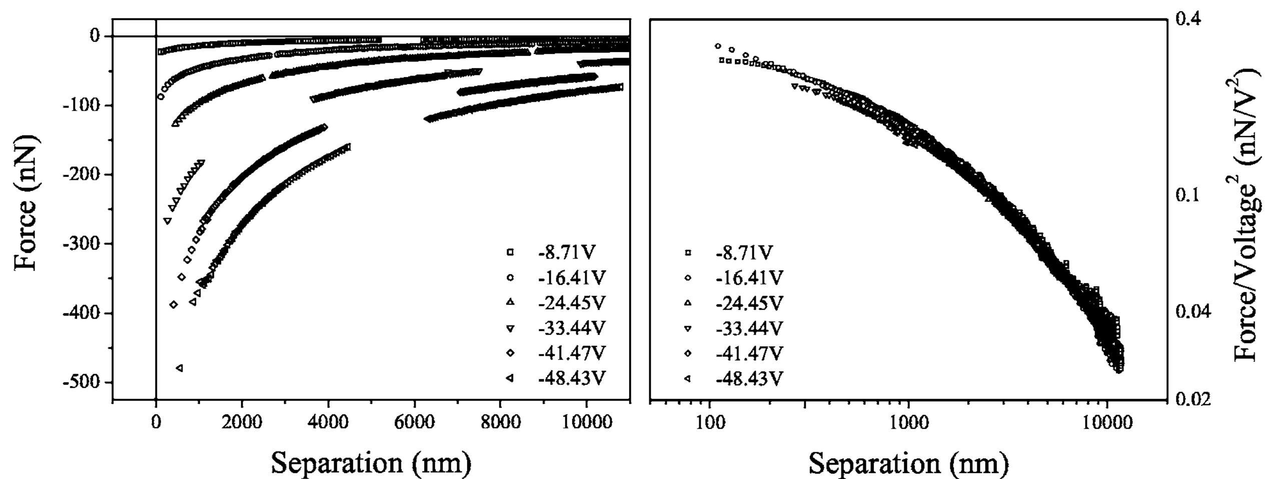

FIG. 6. Left side: set of six force versus separation curves acquired by applying six different voltages between a Cr/Au coated triangular cantilever (L=116 μm, w=32 μm, t_c=0.6 μm, K=0.33 N/m) with pyramidal tip (R=160 nm, H=2.2 μm) and a Cr/Au coated surface. We started at −48.43 V, and decreased the voltages stepwise. The data points missing are due to the measurement technique and the not so perfect synchronization between piezo scan and applied voltrage frequencies. Right side: Each of the six force curves was divided by the square of the applied voltage. The representation is in the log/log scale, therefore the sign of the force was changed from negative to positive.

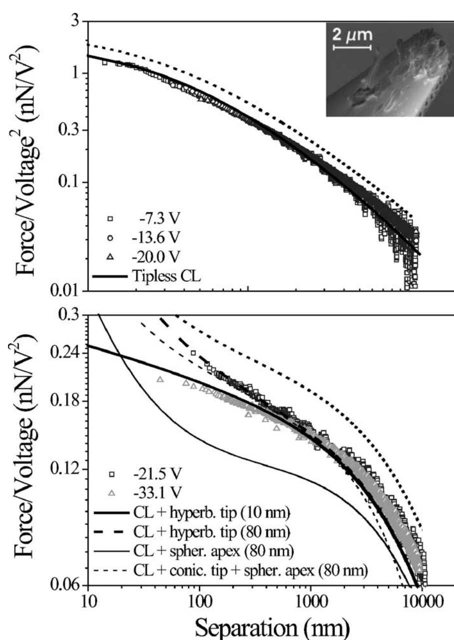

FIG. 7. Plot of F/V^2 versus separation in log/log scale for a triangular Cr/Au coated cantilever (Top: $L=114$ μm, $w=42$ μm), and for a rectangular silicon cantilever (Bottom: $L=470$ μm, $w=50$ μm, $t_c=2.1$ μm, $K=0.238$ N/m). Different voltages were applied and different piezo scan lengths were tested. Black lines represent the calculations employing the cantilever and tip parameters determined from optical microscopy and SEM images, and the correction function $h(Z_0,L',\tan\beta)$. Top: $H_{\text{debris}}\cong 0.3$ μm, $\beta=15°$; Bottom: $H=12.5$ μm, $\beta=4.5°$, $\theta=35°$). The dotted curves in both graphs are calculations considering $h(Z_0,L',\tan\beta)=1$.

copy and SEM images: Experiment and calculation are in good agreement. If instead $h=1$ was used, i.e., the correction function was ignored, we obtained a much larger force, corresponding to the dotted line. In the calculation we had to utilize a tip height of 0.3 μm, despite the fact that the cantilever was tipless. This was clarified by the SEM images of the cantilever after the experiments, which showed some nanoscopic ″debris″ sticking to the cantilever. This might be due to some dirt picked up during the force measurements, or most probably to delamination of the Cr/Au coating of the cantilever as the result of the high applied voltages (inset of upper graph). In the lower graph we show experiments where we used a rectangular cantilever with a quasiconical tip, like the one shown in Fig. 5. The force curves were acquired at different voltages and by using different piezoscan ranges (here only the 12 μm scans are shown). They again confirm the V_0^2 dependence. The curve represented with open triangles was the first in the experimental series, acquired with an unused cantilever. Thus its tip was very sharp tip ($R \leqslant 10$ nm). Each further acquired force curve causes blunting of the tip, which becomes clear from the curve represented with open circles. In that case the tip radius was larger ($R \approx 70$ nm). The solid and dashed thick lines show calculations of the force according to Eqs. (21) and (5). When we used Eqs. (3) and (4) instead of Eq. (5) for the tips, we obtained less accurate results (solid and dashed thin lines, respectively). The parameters for $h(Z_0,L',\beta)$ were again obtained from optical microscopy and SEM images. Also in this case, if we put $h=1$, we obtained a much larger force, corresponding to the dotted line.

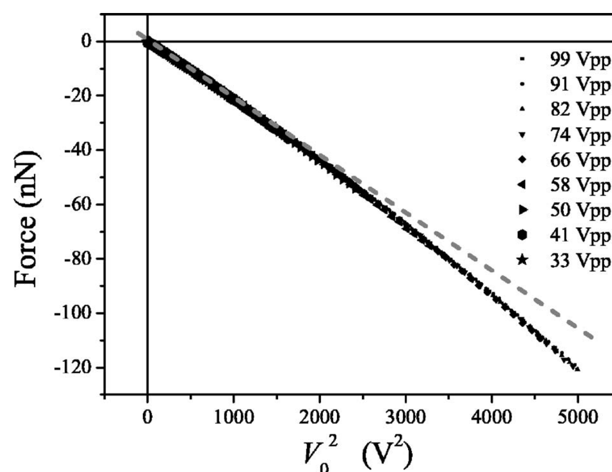

FIG. 8. V_0^2 dependence of the electrostatic force acting on a triangular cantilever ($L=190$ μm, $w=20$ μm, $t_c=0.69$ μm, $K=0.072$ N/m). The distance between cantilever and surface was about 12.0 μm, the inclination of the cantilever with respect to the surface was about $\beta=10°$, and triangular ac voltages were applied. The dashed gray line represents a linear fit to the force data until up to about 1600 V^2.

Summarizing, we were able to describe force curves of triangular and rectangular, with tip and tipless, cantilevers using the correction function $h(Z_0,L',\beta)$. The force calculated using Eq. (3), the spherical apex, is deficient over the whole range of separations. This is expected, since we assume the apex directly on the cantilever, while it should sit on an ideal rod having the same length as the tip. The force calculated using Eq. (4), the conical tip with spherical apex, describes the force accurately for separations smaller than 1000 nm, but fails at larger separations. The most accurate force calculation is given by Eq. (5), the hyperboloid tip with spherical apex, by which we are able to describe the experimental curves over the entire separation range.

To determine the range in which the electrostatic force is proportional to V_0^2, force curves were acquired by keeping the piezo extension constant, and by applying triangular voltages of different magnitudes between the cantilever and surface. In one experiment, represented in Fig. 8, we varied the voltage between 33 and 99 $V_{\text{peak-peak}}$, the initial separation between the cantilever and surface being about 12 μm. All forces overlap, higher voltages generating larger forces. Forces are represented only up to about 120 nN, because this is the maximal range of the detector. This corresponds to $V_0^2 \cong 5000$ V^2, corresponding to a voltage of about 70 $V_{\text{peak-peak}}$. One can observe a slight deviation from the linear behavior (dashed gray line) with increasing voltages, starting from about 1600 V^2. This might be a hint of a nonlinear behavior of either the detector, or it might be due to the fact that we are not anymore in the "small deflections" approximation where the cantilever can be treated as an ideal spring.

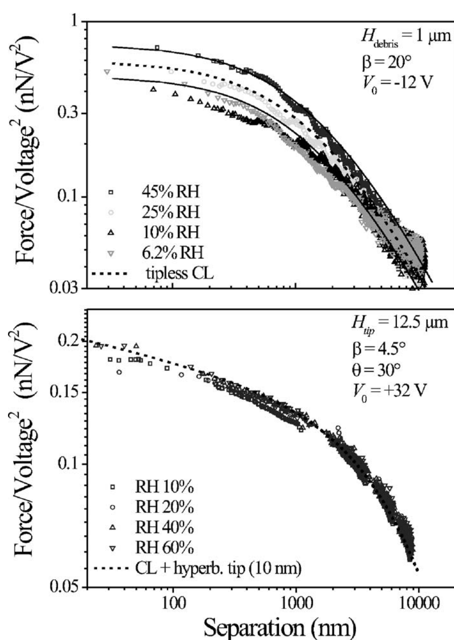

FIG. 9. RH dependence of a cantilever bending: F/V^2 versus separation plots in the log/log scale. Top: triangular, tipless cantilever, Cr/Au coated on both sides ($L=192$ μm, $w=36$ μm, $t_c=0.75$ μm, $K=0.135$ N/m). Bottom: rectangular, uncoated silicon cantilever with tip ($L=475$ μm, $w=50$ μm, $t_c=2.1$ μm, $K=0.243$ N/m). The dashed lines in both graphs represent the calculated force curves according to Eqs. (21) and (5), utilizing the specified parameters.

B. Change of the relative humidity

Using a cantilever coated with a Cr/Au layer, the force increased with increasing RH, irrespective of the changed direction of RH (Fig. 9, upper graph). Using an uncoated silicon cantilever, the force did not change with RH (lower graph). There is, in fact, no physical reason for the electrostatic force to be influenced by the RH, though it is known that the RH affects the breakdown field strength in the gap between two electrodes.[39] We have at this point no explanation for the RH dependence. A tentative explanation could be that the exposed parts of the Cr/Au layers along the edges of the cantilever form a battery. In fact, both metals are equally exposed to the humid air, because the Au layer does not encapsulate the Cr layer completely, but leaves the edges free. Since Cr and Au have redox potentials, respectively, of about −0.9 and +1.5 V, the equivalent voltage is about 2.4 V, but it might be tuned by the thickness of the adsorbed water layer, which is, in turn, influenced by RH. This additional voltage could change the surface tension on one side of the cantilever. In the upper graph, the two solid lines enclose the region of forces calculated by changing the applied voltage $V_0=-12$ V by ±1.2 V. The measured forces only partially lie within this region, which signifies that also other factors might affect the RH-dependent bending. In the lower graph and for the silicon cantilever, the forces are calculated for a cantilever with a hyperboloid tip. The measured forces are best described by curves calculated using $R=10$ nm, close to the value determined by SEM.

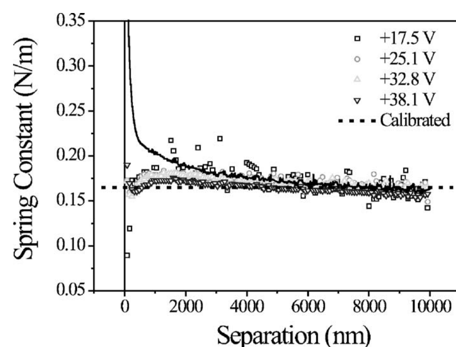

FIG. 10. Graph of the spring constant K plotted versus cantilever-surface separation. Cantilever properties are $L=470$ μm, $w=50$ μm, $R=50$ nm, $H=12.4$ μm, $\beta=4°$, $\theta=30°$. The experimental deflection curves were acquired at the voltages indicated in the legend. The dashed black line represents the spring constant determined with the thermal noise method. The continuous black line represents a calculation made by assuming a wrong R.

C. Spring constant calibration

It is possible to benefit from the well-defined and tunable electric force for the purpose of calibrating the spring constant of AFM cantilevers (Fig. 10). Suppose the spring constant K is unknown: Upon acquiring an experimental curve, we would not be able to convert the cantilever deflection into a force. We could calculate, however, the electrostatic force acting on the cantilever using Eqs. (3)–(5) and (21), like we showed above, since we know all the parameters from optical microscopy and SEM images. K is then simply obtained by dividing the calculated force F by the measured deflection, point by point, for the whole separation range. The values for four voltages (see figure legend) are presented in the graph. The higher voltage provides a smoother curve while the lower voltage provides a more noisy curve. The mean values of the curves for the applied voltages of +17.5, +25.1, 32.8, and 38.1 V are, respectively, $K=0.171$ (±0.017), 0.172 (±0.020), 0.172 (±0.019), and 0.166 (±0.023) N/m. The value determined by the thermal noise method is $K=0.165$ (±0.004) N/m. Depending on the applied voltage, we thus commit an error between 1% and 5% for this particular cantilever. One advantage is intrinsic to this method: by definition, K must be a constant over the whole separation range, therefore the curves should be close to horizontal lines. If they are not, then one or more of the cantilever parameters in Eqs. (3)–(5) and (12) must be wrong. To show this, we used, for example, a different value for R, 500 instead of 50 nm. As is evident from the graph, the curve is not even nearly horizontal, K appearing to increase at small separations, which cannot be. We estimated spring constants for five more cantilevers, triangular and rectangular, tipless and with tip, and the agreement between values calculated with the present method and calibrated with the thermal noise method was within 20% for all (results are not shown here).

V. CONCLUSION

We have quantitatively compared existing models for the electrostatic force acting between a cantilever and a flat sur-

face in AFM with a large number of experiments using triangular and rectangular cantilevers, with and without tip, with and without metal coating, and at different experimental conditions of temperature and RH. We introduced a correction function $h(Z_0, L', \beta)$ for the cantilever contribution to the overall electrostatic force, which is due to (i) geometrical considerations, (ii) the calibration procedure common in AFM force spectroscopy, and (iii) the different action of the electrostatic force on the cantilever (uniformly distributed load) and on the tip (concentrated load). We used a method for applying a voltage (rectangular half-wave) in order to get rid of voltage-independent contributions to the electrostatic force. The dependence of the electrostatic force on the square of the applied voltage for all considered cases was confirmed. For metal coated cantilevers the electrostatic force increases with increasing RH, while this is not the case for uncoated cantilevers. Finally, we showed that the electrostatic force acting on a cantilever can be employed for calibrating cantilever spring constants with an accuracy comparable to other established calibration procedures.

ACKNOWLEDGMENTS

We thank Gunnar Glaßer, Uwe Rietzler, Maren Müller for SEM images; Stefan Kahle, Stefan Weber, Andreas Best, and Arkadiusz Ptak for discussions; Michael Kappl for the force curve data analysis software. We acknowledge financial support by the Deutsche Forschungsgemeinschaft (DFG Grants No. Bu 701/19 and No. HA 2696/2-2).

*Author to whom correspondence should be addressed. Email address: bonaccur@mpip-mainz.mpg.de

[1] G. Binnig, H. Rohrer, C. Gerber, and E. Weibel, Phys. Rev. Lett. **49**, 57 (1982).
[2] G. Binnig, C. F. Quate, and C. Gerber, Phys. Rev. Lett. **56**, 930 (1986).
[3] D. M. Eigler and E. K. Schweizer, Nature (London) **344**, 524 (1990).
[4] Y. Martin, D. W. Abraham, and H. K. Wickramasinghe, Appl. Phys. Lett. **52**, 1103 (1988).
[5] A. Olbrich, B. Ebersberger, and C. Boit, Appl. Phys. Lett. **73**, 3114 (1998).
[6] J. M. R. Weaver and D. W. Abraham, J. Vac. Sci. Technol. B **9**, 1559 (1991).
[7] J. E. Stern, B. D. Terris, and H. J. Mamin, Appl. Phys. Lett. **53**, 2717 (1988).
[8] B. D. Terris, J. E. Stern, D. Rugar, and H. J. Mamin, Phys. Rev. Lett. **63**, 2669 (1989).
[9] C. Böhm, C. Roths, and U. Müller, Mater. Sci. Eng., B **24**, 218 (1994).
[10] J. Hu, X. D. Xiao, and M. Salmeron, Appl. Phys. Lett. **67**, 476 (1995).
[11] S. Jegadesan, R. C. Advinicula, and S. Valiyaveettil, Adv. Mater. (Weinheim, Ger.) **17**, 1282 (2005).
[12] D. Wouters, R. Willems, and S. Hoeppener, Adv. Funct. Mater. **15**, 938 (2005).
[13] M. Guggisberg, M. Bammerlin, C. Loppacher, O. Pfeiffer, A. Abdurixit, V. Barwich, R. Bennewitz, A. Baratoff, E. Meyer, and H. J. Guntherodt, Phys. Rev. B **61**, 11151 (2000).
[14] R. Erlandsson, G. M. McClelland, and C. M. Mate, J. Vac. Sci. Technol. A **6**, 266 (1988).
[15] H. W. Hao, A. M. Baro, and J. J. Saenz, J. Vac. Sci. Technol. B **9**, 1323 (1991).
[16] L. Boyer, F. Houze, and A. Tonck, J. Phys. D **27**, 1504 (1994).
[17] S. Hudlet, M. Saint Jean, B. Roulet *et al.*, J. Appl. Phys. **77**, 3308 (1995).
[18] S. Belaidi, P. Girard, and G. Leveque, J. Appl. Phys. **81**, 1023 (1997).
[19] S. Hudlet, M. Saint Jean, and C. Guthmann, Eur. Phys. J. B **2**, 5 (1998).
[20] M. Saint Jean, S. Hudlet, and C. Guthmann, J. Appl. Phys. **86**, 5245 (1999).
[21] G. Koley, M. G. Spencer, and H. R. Bhangale, Appl. Phys. Lett. **79**, 545 (2001).
[22] S. Gomez-Monivas, L. S. Froufe, and R. Carminati, Nanotechnology **12**, 496 (2001).
[23] J. Colchero, A. Gil, and A. M. Baro, Phys. Rev. B **64**, 245403 (2001).
[24] B. M. Law and F. Rieutord, Phys. Rev. B **66**, 035402 (2002).
[25] G. M. Sacha and J. J. Saenz, Appl. Phys. Lett. **85**, 2610 (2004).
[26] G. M. Sacha, A. Verdaguer, J. Martinez *et al.*, Appl. Phys. Lett. **86**, 123101 (2005).
[27] An accidental error must have been made in the representation of the force data in Fig. 7, whereas the maximal range of tip-sample separations achievable by the AFM used by the authors (Autoprobe CP, Park Instruments) is only 7500 nm (See datasheet of the instrument at http://www.veeco.com/html/datasheet_cp).
[28] N. N. Burnham, X. Chen, and C. S. Hodges, Nanotechnology **14**, 1 (2003).
[29] J. J. Saenz and R. Garcia, Appl. Phys. Lett. **65**, 3022 (1994).
[30] S. A. C. Gould, B. Drake, and C. B. Prater, Ultramicroscopy **33**, 93 (1990).
[31] D. R. Evans and V. S. J. Craig, J. Phys. Chem. B **110**, 5450 (2006).
[32] H.-J. Butt, B. Cappella, and M. Kappl, Surf. Sci. Rep. **59**, 1 (2005).
[33] From the "beam mechanics section" of Enginering Fundamentals (http://www.efunda.com).
[34] J. E. Sader, Rev. Sci. Instrum. **66**, 4583 (1995).
[35] J. L. Hutter, Langmuir **21**, 2630 (2005).
[36] S. Ecke, R. Raiteri, and E. Bonaccurso, Rev. Sci. Instrum. **72**, 4164 (2001).
[37] H.-J. Butt and M. Jaschke, Nanotechnology **6**, 1 (1995).
[38] J. L. Hutter and J. Bechhoefer, Rev. Sci. Instrum. **64**, 1868 (1993).
[39] K. Feser, Bulletin ASE **63**, 278 (1972).